ACSNANO

www.acsnano.org

ARTICLE

3D Freestanding DNA Nanostructure Hybrid as a Low-Density High-Strength Material

Feng Zhou, Wei Sun, Chen Zhang, Jie Shen, Peng Yin,* and Haitao Liu*

Cite This: https://dx.doi.org/10.1021/acsnano.0c00178

Read Online

ACCESS | Metrics & More | Article Recommendations | Supporting Information

ABSTRACT: Structural DNA nanotechnology can produce a wide range of 3D nanostructures with programmable structure and size at <5 nm resolution. However, it is challenging to dry these structures without capillary force-induced damage. As a result, the applications of 3D DNA nanostructures have long been limited in aqueous environments. Ready access to free-standing 3D DNA nanostructures in the dry state could revolutionize many research areas, especially in the development of low-density, high-strength materials. Here we report a method to obtain free-standing wireframe 3D DNA tetrahedra in air on a solid substrate, such as SiO_2 and mica, by absorbing uranyl acetate and lyophilization. The dried DNA tetrahedron structure, 93 ± 2 nm in height, withstands 42 ± 22 nN of loading force. The effective hardness (9.1 ± 5.1 MPa) and Young's modulus (77 ± 48 MPa) of this low-density (70.7 kg/m^3) DNA-inorganic hybrid nanostructure are comparable to other reported low-density high-strength materials.

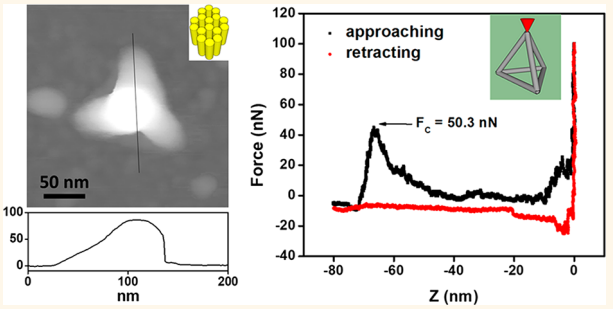

KEYWORDS: *free-standing, 3D DNA nanostructure, uranyl acetate, lyophilization, high strength, indentation*

Tremendous efforts have been made to create synthetic materials and structures that are of both low density and high mechanical strength. Such materials are key to the continuing weight reduction of cars, airplanes, and spacecrafts. For bulk materials, strength is correlated with density; as a result, lowering the density can drastically impair the mechanical properties.[1−4] Various approaches have been made to address this challenge.[5−16] Among them, one promising solution is to design micro- or nanoscale hierarchy structures, as has been demonstrated in mechanical metamaterials,[5] metallic microlattices,[6,7] ceramic composite trusses,[8] ceramic nanolattices,[10] carbon fiber-reinforced polymer lattices,[12] and TiN nanotrusses.[14,15] Polymer- and metal-based hierarchical structures have been fabricated by dual-beam photolithography; these materials showed very high strength (modulus ∼200 MPa) at low density (<100 kg/m^3).[10] However, with the exception of surface coating,[8] the critical features of these hierarchical structures are currently limited at micrometer scales. The mechanical property of nanoscale hierarchical structures is largely unexplored.

DNA nanotechnology is able to produce a wide range of nanostructures with programmable structure and size at atomic resolution.[17−32] Complex shaped lattices,[20,21,25,26] containers,[33] curvatures,[24] wireframes,[34,35] hollow polyhedra,[27,36−38] frameworks,[28,30,31,39,40] crystals,[22,32] and nanomachines[41] have been reported using DNA as building blocks. Among those nanostructures, hollow DNA polyhedra, with their wireframe-based construction, best mimic the structure of many known mechanical metamaterials. Therefore, such programmable DNA nanostructures could serve as a model system to understand the 3D architecture−mechanical property relationship of low-density materials.

However, 3D DNA nanostructures are soft materials, and their applications have long been limited to aqueous environments. An individual double helix can be pulled apart by unzipping with a force of about 10 to 15 piconewton (pN) or partially untwisted after being stretched under 60 pN of force.[42] A 3D DNA nanostructure, such as DNA polyhedra, nanopillars, and hierarchical structures, deforms irreversibly with a threshold force of tens to hundreds of pN in buffer solutions.[28,31,35,43] Fan and his co-workers showed that by silicification of the DNA origami nanostructure, the DNA tetrahedron could withstand 1 nN of force without obvious change of shape, while the structure was bent at a load of 3.0 nN in the buffer.[44]

The weak mechanical properties of 3D DNA nanostructures make them prone to damage during the drying process. A hollow 3D DNA structure cannot withstand the strong capillary forces

Received: January 7, 2020
Accepted: May 1, 2020
Published: May 1, 2020

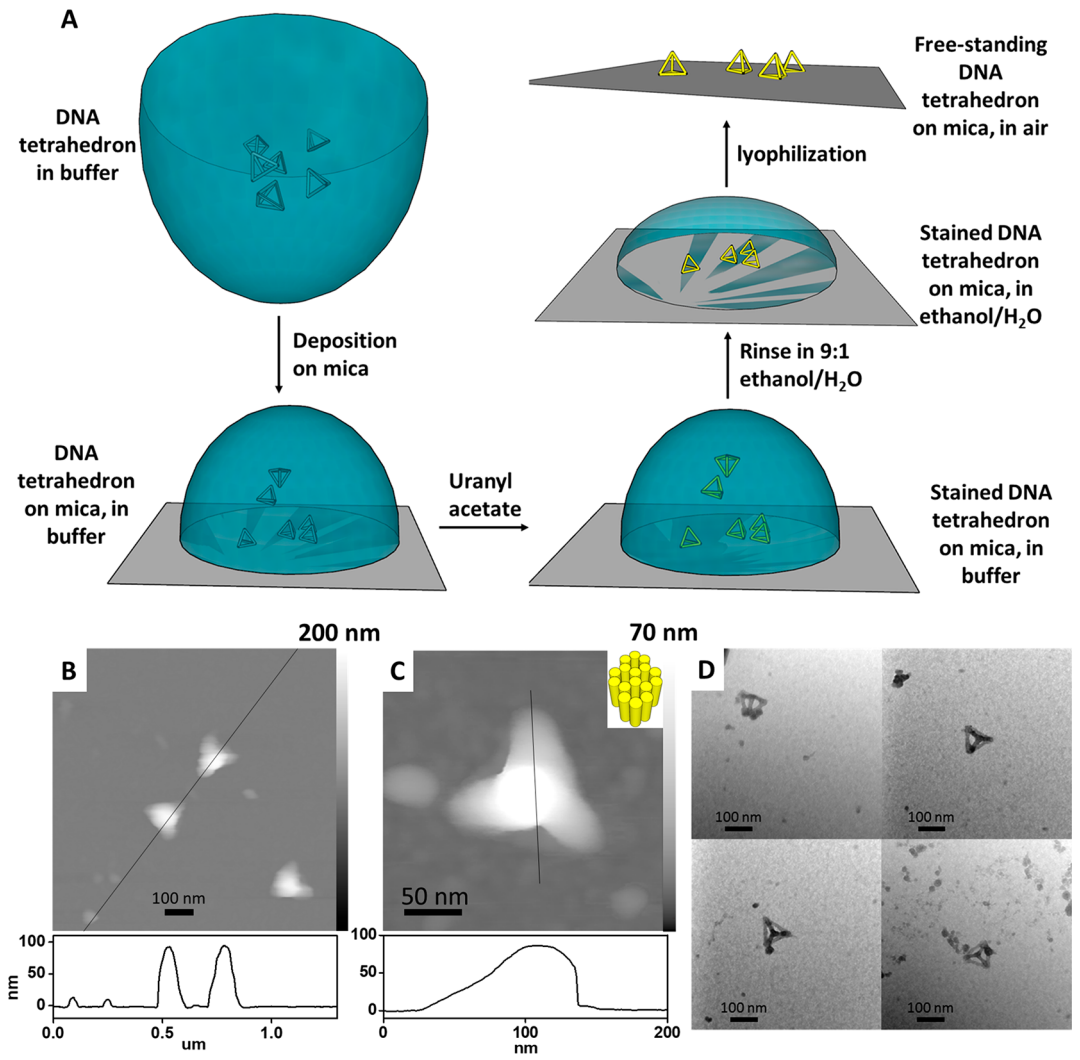

Figure 1. (A) Schematics of the preparation of free-standing DNA tetrahedra in air. (B) Representative AFM image (top) and cross-sectional analysis (bottom) of the DNA tetrahedron deposited on mica in air. (C) High-resolution AFM image (top) and cross section profile (bottom) showing the fine structure of the DNA tetrahedron. Cylinder model (inset) illustrates the cross-section structure of each arm of the tetrahedron. (D) TEM bright-field images of free-standing DNA tetrahedra deposited on a SiO_2 grid.

or transverse sheer forces; upon drying, these structures inevitably collapse or rupture.[39,44] Due to this reason, the characterization of hollow 3D structures of DNA have been largely limited to specialized methods, such as cyro-EM[30,33,36−38,40] and super-resolution fluorescence microscopy,[27] that can probe the structure in aqueous solution. Recent work showed that DNA-origami-templated silicification could generate free-standing 3D origami crystals in air,[45] but the diameter of each building strut was increased by 28%.

Here we report a simple and robust method to obtain a free-standing 3D low-density DNA nanostructure on a solid substrate, such as SiO_2 and mica. We show that by absorbing uranyl acetate onto a DNA frame followed by lyophilization, a free-standing 3D hollow DNA nanostructure can be obtained in air. The free-standing 3D hollow DNA nanostructure was characterized by tapping mode atomic force microscopy (AFM) in air as well as transmission electron microscopy (TEM). The mechanical properties of the 3D hollow DNA nanostructure were studied by AFM indentation. We found that the DNA nanostructures show surprisingly high mechanical strength. The collapsing force (42 ± 22 nN (N = 53)) was 2−3 orders of magnitude higher than the corresponding values of unstained DNA tetrahedra and DNA nanopillars[28,43] (both measured in solution), or the simulated force response[31] of DNA molds, and a 14-fold increase compared to the force that caused irreversible damage to the silica-coated tetrahedral DNA origami nanostructure in water.[44] The effective hardness (9.1 ± 5.1 MPa (N = 53)) and Young's modulus (77 ± 48 MPa (N = 53)) of this low-density (70.7 kg/m^3 (see SI for details)) DNA structure are comparable to the reported ceramic nanolattices,[10] nanotubular bulk materials,[16] and foams.[46]

RESULTS AND DISCUSSION

A DNA tetrahedron, with a dimension of 100 nm in length and 12 nm in thickness for each rod-like arm, was synthesized by self-assembly of DNA tripods.[27] During the solvent evaporation, the DNA nanostructure pins the solid−liquid−air interface and the capillary force exerts a downward pressure onto the nanostructure, causing mechanical damage (Figure S1). Using the surface tension of the solvent (water−ethanol mixture) and the dimensions of the DNA nanostructure, we estimate that the capillary force experienced by the DNA tetrahedron nanostructure is on the order of 4 nN (see SI for detailed calculations). Given the simplicity of the model, this value should be regarded

https://dx.doi.org/10.1021/acsnano.0c00178
ACS Nano XXXX, XXX, XXX−XXX

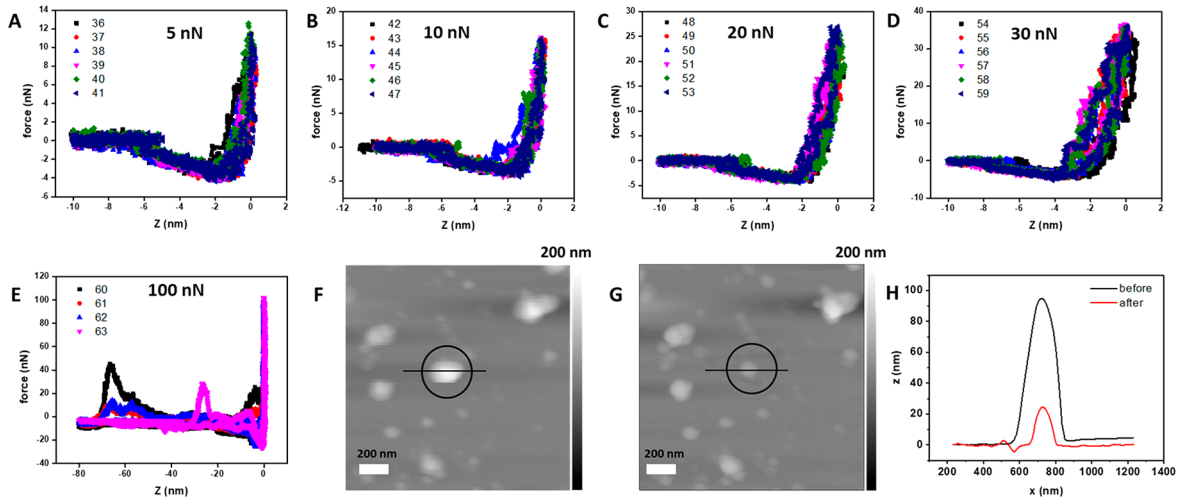

Figure 2. Indentation study of free-standing DNA tetrahedron. Compiled approaching and retracting force curves of a DNA tetrahedron after repeated indentations capped at (A) 5 nN, (B) 10 nN, (C) 20 nN, (D) 30 nN, and (E) 100 nN showing the reversible (A–C) and irreversible (E) compression process. The labeling inside each figure indicates the sequence of indentation experiments. Note: The force threshold cap was defined relative to the initial force value measured at *ca.* $z = -200$ nm. The AFM images of a DNA tetrahedron (F) before and (G) after all the indentation experiments show the change of topography of the same DNA tetrahedron (circled). (H) Cross-sectional analysis of the DNA tetrahedron before and after indentation experiments showing the decrease of height after irreversible indentation on the nanostructure.

as a lower bound, order of magnitude estimation of the force that an individual DNA nanostructure needs to overcome. Thus, the stabilization of a 3D DNA wireframe hollow nanostructure requires efforts on either enhancing the mechanical properties of the 3D architectures or reducing the capillary force during drying, or both.

Lyophilization is a known technique that can reduce capillary force damage because it eliminates the liquid–vapor interface that is typically present during solvent removal. In a separate work, we observed that uranyl acetate can form dense coatings on the DNA nanostructure. These results motivated our initial exploration of free-standing DNA nanostructures in the dry state. We prepared free-standing hollow DNA tetrahedron structures in dry state by uranyl acetate absorption followed by freeze-drying (Figure 1A). Tetrahedron structures, with a lateral length of 158 ± 5 nm and height of 93 ± 2 nm ($N = 20$), were found in the tapping mode AFM images (Figures 1B,C and S2). The dimension of these structures matches that of the free-standing DNA tetrahedron (expected length: 100 nm, expected height: 82 nm; note that the length measured by AFM will be larger than the real values due to the tip-convolution effect), indicating that the DNA tetrahedra did not collapse. Additionally, the bright-field TEM images showed that only the wireframe of the DNA nanostructures has been stained by UO_2^{2+}; the interior volume of the DNA tetrahedron nanostructure is free of inorganic residue. The edge of the DNA tetrahedron measured by TEM is 100 ± 6 nm with a thickness (fwhm) of 11.5 ± 2.2 nm (Figures 1D and S3). We conclude that the UO_2^{2+} stain did not compromise the fidelity of the DNA nanostructure and significantly improved its mechanical stability.

We found that both the adsorption of UO_2^{2+} and the freeze-drying were needed to obtain the free-standing structure. In a control experiment, we freeze-dried the DNA nanostructure without UO_2^{2+} staining and found the structures collapsed (Figure S4A). Uranyl ions (UO_2^{2+}) bind to phosphate groups in DNA.[47] We suspect that the absorbed UO_2^{2+} ions increase the mechanical stability of the DNA nanostructure through their ionic interaction with the neighboring phosphates, effectively creating a thin layer of uranyl phosphate coating on the DNA surface. In another control experiment, we dried the stained DNA sample using a stream of N_2 instead of freeze-drying. AFM imaging showed that the DNA nanostructures collapsed, as the height was reduced to 24 ± 5 nm (Figure S4B). Furthermore, the thickness of each rod in the free-standing DNA nanostructure (11.5 ± 2.2 nm) was the same as that of the regular stained DNA tetrahedra (11.4 ± 1.2 nm),[27] indicating that lyophilization shielded the hollow 3D DNA nanostructure from the surface-tension-induced damage without compromising its structural features.

We have characterized the mechanical properties of the free-standing DNA nanostructure in air using AFM indentation. In a typical experiment, a tapping mode AFM scan was first conducted to locate the free-standing DNA nanostructures. The same AFM tip was then placed over a DNA nanostructure and force–distance curves were measured at the same spot at various force thresholds from 5 nN to 300 nN. Due to the difficulty of achieving precise tip placement on the nanostructure, we conducted successful indentations on two different samples. We found that the approaching and retracting force curves overlapped at force threshold from 5 to 20 nN (Figures 2A–C and S5), indicating that the structure remained intact and stationary, at least for 6 cycles of indentation. When the threshold increased to 30 nN (Figure 2D), the first 6 cycles of indentation showed identical curves, indicating the absence of any long-term plastic deformation. However, in this case, the approaching and retracting curves did not overlap (*ca.* 2 nm of deviation), suggesting the presence of elastic deformation that did not restore within the same cycle.

When the force threshold was increased to 100 nN (Figure 2E), a feature consistent with structural collapse was found in the first force curve (black). In this case, the force response showed an approximate linear increase within the initial *ca.* 5 nm of contacting the tetrahedron. This linear region was followed by a sudden decrease in the force at *ca.* 45 nN, which we attributed to the collapse of the hollow DNA tetrahedron. After an additional 65 nm of displacement, the force response showed another steep increase before reaching the setoff force of 100

https://dx.doi.org/10.1021/acsnano.0c00178
ACS Nano XXXX, XXX, XXX–XXX

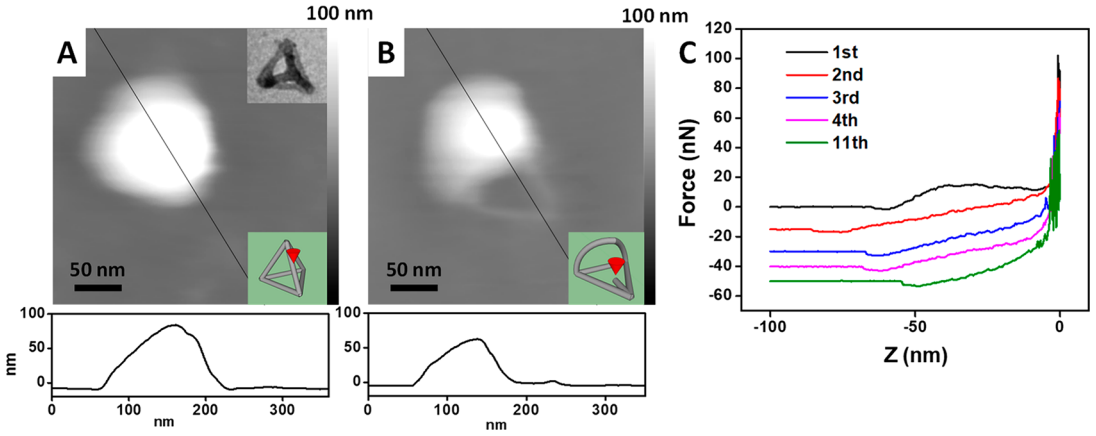

Figure 3. Indentation experiments on an individual DNA tetrahedral structure. AFM image and cross-sectional analysis of a free-standing DNA tetrahedron (A) before and (B) after indentation experiments. (C) Multiple cycles of force−distance curves of a DNA tetrahedron measured on the same spot. The cartoon insets in A and B represent the relative location between the AFM tip and free-standing tetrahedron.

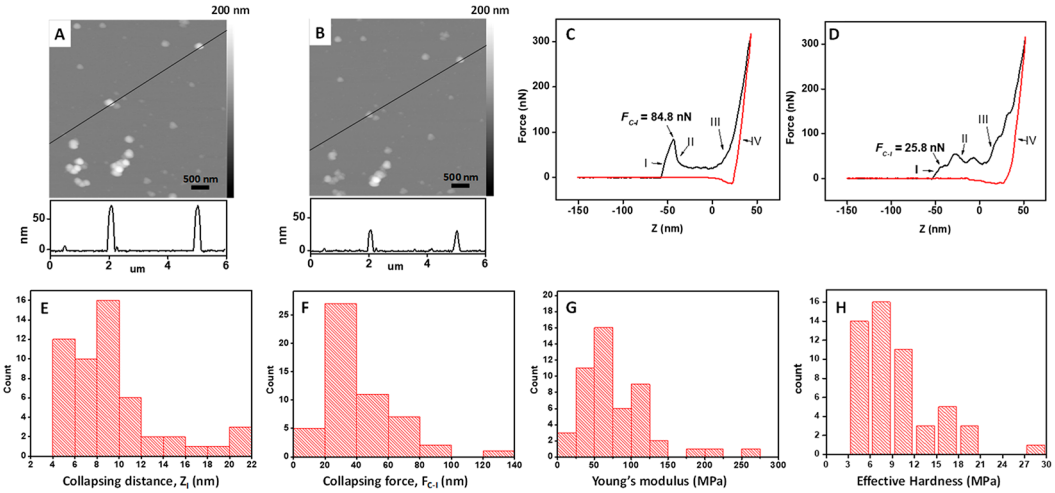

Figure 4. Indentation experiments of free-standing DNA tetrahedra *via* force mapping. AFM images and cross-sectional analysis of free-standing DNA tetrahedra before (A) and after (B) force mapping showed a decrease in the height of DNA nanostructure after the force mapping. (C and D) Representative force curves of DNA tetrahedra showing single and multiple stages in the structural collapse. Statistics of (E) displacement before collapse (*i.e.*, from the contact to the onset of plastic deformation), Z_I, (F) collapsing force at the first breakage point, F_{C-I}, (G) Young's modulus, *E*, and (H) effective hardness of free-standing DNA tetrahedra.

nN, indicating that the AFM tip had reached the supporting substrate. The total indentation depth (*ca.* 80 nm) is smaller than the height of the nanostructure (95 nm, Figure 2F and H), suggesting that the AFM tip was not placed at the apex of the DNA nanostructure and most likely a partial collapsed occurred. In the following cycles of indentation (red, blue, and pink), similar collapsing behavior was observed, although each cycle showed some variations from the previous one; the collapsing force also became smaller and the AFM tip needed additional travel to reach the DNA nanostructure, suggesting that the indentation-induced deformation was progressive and irreversible. After all the indentation experiments, the tapping mode AFM image taken at the same location showed that the height of the DNA nanostructure decreased from 95 nm to 25 nm (Figure 2G and H). The height of the collapsed structure is comparable to that of the collapsed structure we obtained without using freeze-drying (24 nm, see Figure S4B).

We observed very similar behaviors (reversible compression at low force, irreversible collapsing at high force) on a different DNA tetrahedron (Figure S6). In this case, we observed overlapping approaching and retracting force curves when the force threshold was 10 and 20 nN. The effective Young's modulus of the stained tetrahedron was calculated using the reversible force curve and using the surface area covered by the DNA tetrahedron (4330 nm^2). The calculated Young's modulus varied depending on the force threshold, placement of tip on the DNA nanostructure, and the indentation rate. The Young's moduli of the two samples were 230 ± 64 MPa (based on 18 curves measured on the sample shown in Figure 2A−C) and 162 ± 29 MPa (based on 12 curves in Figure S6A,B).

Figure 3 shows the indentation experiment on another tetrahedron structure (Figure 3A), in which the force threshold was set as 100 nN to collapse the nanostructure in the first indentation. The first force curve exhibited the same collapsing behavior, while that was not observed upon repeated indentations on the same location, indicating that plastic deformation occurred (Figure 3C). We used tapping-mode AFM to characterize the DNA nanostructure before and after indentation (Figure 3A and 3B). In this case, we found that the height of the tetrahedron decreased from 89 nm to 62 nm and a triangular base (6−8 nm in height, Figures 3B and S7) was clearly visible around the partially fractured structure, indicating

https://dx.doi.org/10.1021/acsnano.0c00178
ACS Nano XXXX, XXX, XXX−XXX

that a partial collapse occurred during the indentation. Also shown in Figure S8, the leftover triangular bases after the indentation-induced collapse proved that the standing DNA tetrahedron was indeed hollow.

In addition to these detailed studies on individual structures, we also carried out force mapping to obtain statistics of the mechanical properties. In this experiment, an area having many standing tetrahedra was selected by tapping mode AFM imaging. Afterward, the same AFM tip was used to conduct force mapping of the surface, during which force−distance curves were collected over a 2D array of spots, with a periodicity of 66 nm in both dimensions. The AFM tip was suspended while moving between adjacent spots to prevent contact with the sample other than during the indentation. The force threshold during the force−distance curve measurement was set as 300 nN, which ensured complete collapsing of the DNA tetrahedra. After force mapping, another tapping mode AFM image was collected. We found that the height of many DNA nanostructures in the mapping region decreased to *ca.* 20 nm (Figure 4A and B), consistent with collapse of DNA nanostructures. Out of the 25,600 force curves, we identified 84 that are likely associated with DNA nanostructures, all of which showed the following features (Figure 4C): initial compression with a linear force response (I), collapse and relaxation (II), compression of the collapsed structure (III), and unloading of the AFM tip (IV). In some circumstances, multiple collapses occurred during the indentation, exhibiting multiple peaks in the force curve (Figure 4D), which we attribute to stepwise plastic deformation of the tetrahedron structure. We further reasoned that if the AFM tip was placed on the DNA tetrahedron, the tip displacement between the initial contact and reaching the force threshold should be at least the thickness of two DNA wireframe edges (23 nm). With this additional criterion, we identified 53 indentation results for our statistical analysis below.

The average collapsing force was 42 ± 22 nN (Figure 4F), which was 3 orders of magnitude larger than the DNA nanopillar[43] and a 14-fold increase compared to the force that caused irreversible damage to the silica-coated tetrahedron DNA origami nanostructure in water.[44] The average displacement before the structural collapse (distance between the initial contact and the collapsing point) was 9.1 ± 4.3 nm (Figure 4E). The force response below the collapsing force was 5.2 ± 3.1 nN/nm, which was 2 orders of magnitude larger than the simulated value of the DNA origami box structure (note that the deformations are different: inward for the DNA tetrahedron and outward for the origami box).[31] There was no obvious correlation found between the collapsing force and the collapsing distance. The effective hardness was calculated to be 9.1 ± 5.7 MPa (Figure 4H), and the effective Young's modulus as 77 ± 48 MPa (Figure 4G). The density of the stained nanostructure was calculated to be 70.7 kg/m^3 (see SI for calculation). These characteristics are comparable to those of the ceramic nanolattice structures.[10]

The large variation of the data derived from force mapping is likely due to the random placement of the AFM tip on the DNA nanostructures. In contrast, the variations are much smaller in the data derived from the multiple reversible indentation curves measured on a single DNA nanostructure. The Young's modulus was 230 ± 64 MPa and 162 ± 29 MPa for the samples shown in Figures 2 and S6, respectively.

We estimated the Young's modulus of the individual rod in the stained DNA tetrahedron structure. When the AFM tip was applied on the top apex of the DNA tetrahedron, the collapsing force (F_C) was 32.7 ± 8.1 nN, based on four force−distance curves with a total indentation displacement (the distance between the initial contact and the final point) close to the height of the DNA tetrahedron (93 ± 5 nm). We modeled the individual DNA rod in the wireframe as a buckling column (see SI for details). With these assumptions, the calculated Young's modulus for the individual rod is 15.2 ± 3.8 GPa. Compared to the reported Young's modulus of double-stranded DNAs (100−300 MPa[42,48−50]) or DNA origami nanotubes (75−180 MPa[50]), the individual stained DNA rod in the free-standing DNA tetrahedron is 2 orders of magnitude stronger.

CONCLUSION

We successfully obtained free-standing 3D hollow DNA tetrahedron structure in air by absorbing uranyl acetate on a DNA frame followed by lyophilization. The 3D DNA nanostructure maintained its original morphology, showing minimal structural deformation. The thin coating of uranyl acetate on the DNA frame significantly increased its mechanical properties: at least 2 orders of magnitude higher than the previous measurements collected in water and approaches that of inorganic nanolattice structures. The enhancement of the mechanical properties likely originates from the strong interaction between the phosphate groups in DNA and the UO_2^{2+} ions and thus should broadly apply to other DNA nanostructures. Work is underway to explore if the same effect can be obtained using other cations in place of UO_2^{2+}.

DNA nanotechnology provides rapid access to 3D nanoscale objects. The possibility to use these structures in air may open up new opportunities for both research and applications, in particular, in areas of nanoscale mechanics,[51,52] 3D nanoelectronics,[53] nanoelectromechanical systems, and surface engineering (*e.g.*, wetting control).[54,55] Many of these applications (*e.g.*, omniphobic surface) require both nanoscale and microscale structural features over large areas. Thus, our work also calls for further development of structural DNA nanotechnology to produce larger and more complex 3D DNA nanostructures at reduced cost.

MATERIALS AND METHODS

Preparation of Free-Standing DNA Tetrahedra on Mica. DNA tetrahedra were synthesized following the DNA tripod assembly method.[27] Staple and P8064 scaffold DNAs for preparing the DNA tetrahedral origami were purchased from IDT and Bioneer Corporation, respectively. The unpurified staple DNA strands were mixed with a P8064 scaffold in a molar stoichiometric ratio of 1:1 in 0.5× TEMg buffer (5 mM Tris, pH 7.9, 1 mM EDTA, 12 mM $MgCl_2$). The final concentration of scaffold was adjusted to 10 nM. The mixture was annealed at 80 °C for 15 min, followed by a fast linear cooling step to 65 °C over 75 min and a slow linear cooling step to 24 °C for 70 h. The excess staple DNA was removed by agarose gel purification in an ice−water bath. The as-prepared tetrahedral DNA nanostructure was assembled on a 0.5 × 0.5 cm^2 freshly cleaved mica surface by dripping 5 μL of DNA solution on the substrate and allowed to incubate for 5 min. Then, 2 μL of filtrated 1% uranyl acetate was added on the wet sample and allowed to incubate for 45 s. The substrate was kept in a high-humidity environment during the incubation times. The wet sample was then rinsed with an ethanol−water mixture (v/v: 9:1) several times to remove the extra salt. The wet sample was immersed in liquid N_2 for at least 10 min to freeze the surface and subjected to lyophilization at *ca.* 100 mTorr overnight. The formation of the free-standing DNA tetrahedron has been reproduced in different batches and by different researchers in our lab, independently.

https://dx.doi.org/10.1021/acsnano.0c00178
ACS Nano XXXX, XXX, XXX−XXX

Characterization Methods. *Atomic Force Microscopy.* Surface morphology of DNA tetrahedral structures after drying and mechanical properties of the free-standing DNA tetrahedral structures were characterized by tapping mode AFM and nanoscale indentation using an Asylum MFP-3D AFM equipped with a μmasch NSC15 tip in air.

For indentation data shown in Figure 2, the force distance was set as 200 nm, the setoff force threshold was varied from 5 to 300 nN, and the scan rate was set as 0.1 Hz. For data shown in Figure 3, the force distance was set as 200 nm, the setoff force threshold was 100 nN, and the scan rate was set as 0.99 Hz. In the force mapping experiment, the force distance was set as 200 nm, the setoff force threshold was 300 nN, the scan rate was set as 0.99 Hz, and the distance between adjacent points was set as 67 nm. The force spring constant of the AFM tip was calibrated before the indentation experiments. The calibration process is integrated in the Asylum MFP-3D software, which includes (1) calibration of the inverse of the optical lever sensitivity (InvOLS) to convert the cantilever deflection from volts to meters after performing a force curve on the mica surface; (2) measurement of the thermal power spectral density to determine the resonant frequency of the cantilever; and (3) fitting the first harmonic peak of the cantilever with the calculated InvOLS to calculate the spring constant.

The indentation experiment to measure the mechanical property of the DNA nanostructure included four steps: (1) a prescan using tapping mode AFM to locate a structure of interest; (2) a force-mapping prescan (500 nm scan size, 10 nN threshold) using contact mode AFM to confirm the location of the structure of interest (Figure S9); (3) positioning the AFM tip on the structure to conduct the nanoindentation experiment; (4) a postscan using tapping mode AFM to image the structure of interest.

Transmission Electron Microscopy. A SiO_2 window TEM grid (SO100-A20Q33, SiMPore Inc.) was pretreated with UV/ozone for 2 h to generate a hydrophilic surface. TEM samples were prepared following the same procedure for preparing free-standing DNA tetrahedron structures on mica. TEM was conducted on a JEOL 200CX instrument operated at 200 kV and equipped with a Gatan CCD image system.

ASSOCIATED CONTENT

Supporting Information

The Supporting Information is available free of charge at https://pubs.acs.org/doi/10.1021/acsnano.0c00178.

Additional information (PDF)

AUTHOR INFORMATION

Corresponding Authors

Peng Yin − *Wyss Institute for Biologically Inspired Engineering, Harvard University, Boston, Massachusetts 02115, United States; Department of Systems Biology, Harvard Medical School, Boston, Massachusetts 02115, United States;* orcid.org/0000-0002-2769-6357; Email: peng_yin@hms.harvard.edu

Haitao Liu − *Department of Chemistry, University of Pittsburgh, Pittsburgh, Pennsylvania 15260, United States;* orcid.org/0000-0003-3628-5688; Email: hliu@pitt.edu

Authors

Feng Zhou − *Department of Chemistry, University of Pittsburgh, Pittsburgh, Pennsylvania 15260, United States*

Wei Sun − *Wyss Institute for Biologically Inspired Engineering, Harvard University, Boston, Massachusetts 02115, United States; Department of Systems Biology, Harvard Medical School, Boston, Massachusetts 02115, United States*

Chen Zhang − *Department of Chemistry, University of Pittsburgh, Pittsburgh, Pennsylvania 15260, United States;* orcid.org/0000-0001-5552-1960

Jie Shen − *Wyss Institute for Biologically Inspired Engineering, Harvard University, Boston, Massachusetts 02115, United States; Department of Systems Biology, Harvard Medical School, Boston, Massachusetts 02115, United States*

Complete contact information is available at: https://pubs.acs.org/10.1021/acsnano.0c00178

Notes

The authors declare no competing financial interest.

ACKNOWLEDGMENTS

H.L. acknowledges support from ONR (N000141812555).

REFERENCES

(1) Fan, H.; Hartshorn, C.; Buchheit, T.; Tallant, D.; Assink, R.; Simpson, R.; Kissel, D. J.; Lacks, D. J.; Torquato, S.; Brinker, C. J. Modulus-Density Scaling Behaviour and Framework Architecture of Nanoporous Self-Assembled Silicas. *Nat. Mater.* **2007**, *6*, 418−423.

(2) Qiu, L.; Liu, J. Z.; Chang, S. L. Y.; Wu, Y.; Li, D. Biomimetic Superelastic Graphene-Based Cellular Monoliths. *Nat. Commun.* **2012**, *3*, 1241.

(3) Tillotson, T. M.; Hrubesh, L. W. Transparent Ultralow-Density Silica Aerogels Prepared by a Two-Step Sol-Gel Process. *J. Non-Cryst. Solids* **1992**, *145*, 44−50.

(4) Kim, S.-H.; Kim, H.; Kim, N. J. Brittle Intermetallic Compound Makes Ultrastrong Low-Density Steel with Large Ductility. *Nature* **2015**, *518*, 77−79.

(5) Zheng, X.; Lee, H.; Weisgraber, T. H.; Shusteff, M.; DeOtte, J.; Duoss, E. B.; Kuntz, J. D.; Biener, M. M.; Ge, Q.; Jackson, J. A.; Kucheyev, S. O.; Fang, N. X.; Spadaccini, C. M. Ultralight, Ultrastiff Mechanical Metamaterials. *Science* **2014**, *344*, 1373−1377.

(6) Schaedler, T. A.; Jacobsen, A. J.; Torrents, A.; Sorensen, A. E.; Lian, J.; Greer, J. R.; Valdevit, L.; Carter, W. B. Ultralight Metallic Microlattices. *Science* **2011**, *334*, 962−965.

(7) Torrents, A.; Schaedler, T. A.; Jacobsen, A. J.; Carter, W. B.; Valdevit, L. Characterization of Nickel-Based Microlattice Materials with Structural Hierarchy from the Nanometer to the Millimeter Scale. *Acta Mater.* **2012**, *60*, 3511−3523.

(8) Bauer, J.; Hengsbach, S.; Tesari, I.; Schwaiger, R.; Kraft, O. High-Strength Cellular Ceramic Composites with 3D Microarchitecture. *Proc. Natl. Acad. Sci. U. S. A.* **2014**, *111*, 2453−2458.

(9) Kucheyev, S. O.; Stadermann, M.; Shin, S. J.; Satcher, J. H.; Gammon, S. A.; Letts, S. A.; van Buuren, T.; Hamza, A. V. Super-Compressibility of Ultralow-Density Nanoporous Silica. *Adv. Mater.* **2012**, *24*, 776−780.

(10) Meza, L. R.; Das, S.; Greer, J. R. Strong, Lightweight, and Recoverable Three-Dimensional Ceramic Nanolattices. *Science* **2014**, *345*, 1322−1326.

(11) Kim, K. H.; Oh, Y.; Islam, M. F. Graphene Coating Makes Carbon Nanotube Aerogels Superelastic and Resistant to Fatigue. *Nat. Nanotechnol.* **2012**, *7*, 562−566.

(12) Cheung, K. C.; Gershenfeld, N. Reversibly Assembled Cellular Composite Materials. *Science* **2013**, *341*, 1219−1221.

(13) Worsley, M. A.; Kucheyev, S. O.; Satcher, J. H.; Hamza, A. V.; Baumann, T. F. Mechanically Robust and Electrically Conductive Carbon Nanotube Foams. *Appl. Phys. Lett.* **2009**, *94*, 073115.

(14) Jang, D.; Meza, L. R.; Greer, F.; Greer, J. R. Fabrication and Deformation of Three-Dimensional Hollow Ceramic Nanostructures. *Nat. Mater.* **2013**, *12*, 893−898.

(15) Meza, L.; Greer, J. Mechanical Characterization of Hollow Ceramic Nanolattices. *J. Mater. Sci.* **2014**, *49*, 2496−2508.

(16) Biener, M. M.; Ye, J.; Baumann, T. F.; Wang, Y. M.; Shin, S. J.; Biener, J.; Hamza, A. V. Ultra-Strong and Low-Density Nanotubular Bulk Materials with Tunable Feature Sizes. *Adv. Mater.* **2014**, *26*, 4808−4813.

(17) Chen, J.; Seeman, N. C. Synthesis from DNA of a Molecule with the Connectivity of a Cube. *Nature* **1991**, *350*, 631−633.

https://dx.doi.org/10.1021/acsnano.0c00178
ACS Nano XXXX, XXX, XXX−XXX

(18) Winfree, E.; Liu, F.; Wenzler, L. A.; Seeman, N. C. Design and Self-Assembly of Two-Dimensional DNA Crystals. *Nature* **1998**, *394*, 539−544.
(19) Rothemund, P. W. K.; Papadakis, N.; Winfree, E. Algorithmic Self-Assembly of DNA Sierpinski Triangles. *PLoS Biol.* **2004**, *2*, No. e424.
(20) Rothemund, P. W. K. Folding DNA to Create Nanoscale Shapes and Patterns. *Nature* **2006**, *440*, 297−302.
(21) Douglas, S. M.; Dietz, H.; Liedl, T.; Hogberg, B.; Graf, F.; Shih, W. M. Self-Assembly of DNA into Nanoscale Three-Dimensional Shapes. *Nature* **2009**, *459*, 414−418.
(22) Zheng, J.; Birktoft, J. J.; Chen, Y.; Wang, T.; Sha, R.; Constantinou, P. E.; Ginell, S. L.; Mao, C.; Seeman, N. C. From Molecular to Macroscopic *via* the Rational Design of a Self-Assembled 3D DNA Crystal. *Nature* **2009**, *461*, 74−77.
(23) Linko, V.; Dietz, H. The Enabled State of DNA Nanotechnology. *Curr. Opin. Biotechnol.* **2013**, *24*, 555−561.
(24) Han, D.; Pal, S.; Yang, Y.; Jiang, S.; Nangreave, J.; Liu, Y.; Yan, H. DNA Gridiron Nanostructures Based on Four-Arm Junctions. *Science* **2013**, *339*, 1412−1415.
(25) Ke, Y.; Ong, L. L.; Shih, W. M.; Yin, P. Three-Dimensional Structures Self-Assembled from DNA Bricks. *Science* **2012**, *338*, 1177−1183.
(26) Wei, B.; Dai, M.; Yin, P. Complex Shapes Self-Assembled from Single-Stranded DNA Tiles. *Nature* **2012**, *485*, 623−626.
(27) Iinuma, R.; Ke, Y.; Jungmann, R.; Schlichthaerle, T.; Woehrstein, J. B.; Yin, P. Polyhedra Self-Assembled from DNA Tripods and Characterized with 3D DNA-Paint. *Science* **2014**, *344*, 65−69.
(28) Goodman, R. P.; Schaap, I. A. T.; Tardin, C. F.; Erben, C. M.; Berry, R. M.; Schmidt, C. F.; Turberfield, A. J. Rapid Chiral Assembly of Rigid DNA Building Blocks for Molecular Nanofabrication. *Science* **2005**, *310*, 1661−1665.
(29) Zhang, Y.; Seeman, N. C. Construction of a DNA-Truncated Octahedron. *J. Am. Chem. Soc.* **1994**, *116*, 1661−1669.
(30) Tian, C.; Li, X.; Liu, Z.; Jiang, W.; Wang, G.; Mao, C. Directed Self-Assembly of DNA Tiles into Complex Nanocages. *Angew. Chem.* **2014**, *126*, 8179−8182.
(31) Sun, W.; Boulais, E.; Hakobyan, Y.; Wang, W. L.; Guan, A.; Bathe, M.; Yin, P. Casting Inorganic Structures with DNA Molds. *Science* **2014**, *346*, 1258361.
(32) Ke, Y.; Ong, L. L.; Sun, W.; Song, J.; Dong, M.; Shih, W. M.; Yin, P. DNA Brick Crystals with Prescribed Depths. *Nat. Chem.* **2014**, *6*, 994−1002.
(33) Andersen, E. S.; Dong, M.; Nielsen, M. M.; Jahn, K.; Subramani, R.; Mamdouh, W.; Golas, M. M.; Sander, B.; Stark, H.; Oliveira, C. L. P.; Pedersen, J. S.; Birkedal, V.; Besenbacher, F.; Gothelf, K. V.; Kjems, J. Self-Assembly of a Nanoscale DNA Box with a Controllable Lid. *Nature* **2009**, *459*, 73−76.
(34) Zhang, F.; Jiang, S.; Wu, S.; Li, Y.; Mao, C.; Liu, Y.; Yan, H. Complex Wireframe DNA Origami Nanostructures with Multi-Arm Junction Vertices. *Nat. Nanotechnol.* **2015**, *10*, 779−784.
(35) Weizmann, Y.; Braunschweig, A. B.; Wilner, O. I.; Cheglakov, Z.; Willner, I. A Polycatenated DNA Scaffold for the One-Step Assembly of Hierarchical Nanostructures. *Proc. Natl. Acad. Sci. U. S. A.* **2008**, *105*, 5289−5294.
(36) Zhang, C.; Ko, S. H.; Su, M.; Leng, Y.; Ribbe, A. E.; Jiang, W.; Mao, C. Symmetry Controls the Face Geometry of DNA Polyhedra. *J. Am. Chem. Soc.* **2009**, *131*, 1413−1415.
(37) He, Y.; Ye, T.; Su, M.; Zhang, C.; Ribbe, A. E.; Jiang, W.; Mao, C. Hierarchical Self-Assembly of DNA into Symmetric Supramolecular Polyhedra. *Nature* **2008**, *452*, 198−201.
(38) Shih, W. M.; Quispe, J. D.; Joyce, G. F. A 1.7-Kilobase Single-Stranded DNA That Folds into a Nanoscale Octahedron. *Nature* **2004**, *427*, 618−621.
(39) Smith, D. M.; Schüller, V.; Forthmann, C.; Schreiber, R.; Tinnefeld, P.; Liedl, T. A Structurally Variable Hinged Tetrahedron Framework from DNA Origami. *J. Nucleic Acids* **2011**, *2011* (9), 360954.
(40) Zhang, C.; Su, M.; He, Y.; Zhao, X.; Fang, P.-a.; Ribbe, A. E.; Jiang, W.; Mao, C. Conformational Flexibility Facilitates Self-Assembly of Complex DNA Nanostructures. *Proc. Natl. Acad. Sci. U. S. A.* **2008**, *105*, 10665−10669.
(41) Gerling, T.; Wagenbauer, K. F.; Neuner, A. M.; Dietz, H. Dynamic DNA Devices and Assemblies Formed by Shape-Complementary, Non−Base Pairing 3D Components. *Science* **2015**, *347*, 1446−1452.
(42) Marko, J. F.; Cocco, S. The Micromechanics of DNA. *Phys. World* **2003**, *16*, 37−41.
(43) Kauert, D. J.; Kurth, T.; Liedl, T.; Seidel, R. Direct Mechanical Measurements Reveal the Material Properties of Three-Dimensional DNA Origami. *Nano Lett.* **2011**, *11*, 5558−5563.
(44) Liu, X.; Zhang, F.; Jing, X.; Pan, M.; Liu, P.; Li, W.; Zhu, B.; Li, J.; Chen, H.; Wang, L.; Lin, J.; Liu, Y.; Zhao, D.; Yan, H.; Fan, C. Complex Silica Composite Nanomaterials Templated with DNA Origami. *Nature* **2018**, *559*, 593−598.
(45) Nguyen, L.; Döblinger, M.; Liedl, T.; Heuer-Jungemann, A. DNA-Origami-Templated Silica Growth by Sol−Gel Chemistry. *Angew. Chem., Int. Ed.* **2019**, *58*, 912−916.
(46) Fleck, N. A.; Deshpande, V. S.; Ashby, M. F. Micro-Architectured Materials: Past, Present and Future. *Proc. R. Soc. London, Ser. A* **2010**, *466*, 2495−2516.
(47) Hayat, M. A. *Stains and Cytochemical Methods*; Springer US: New York, 1993; p 362.
(48) Lin, Y.; Shen, X.; Wang, J.; Bao, L.; Zhang, Z.; Pang, D. Measuring Radial Young's Modulus of DNA by Tapping Mode Afm. *Chin. Sci. Bull.* **2007**, *52*, 3189−3192.
(49) Cocco, S.; Marko, J. F.; Monasson, R. Theoretical Models for Single-Molecule DNA and RNA Experiments: From Elasticity to Unzipping. *C. R. Phys.* **2002**, *3*, 569−584.
(50) Li, L.; Liu, L.; Tabata, O.; Li, W. J. Elasticity Measurement of DNA Origami Nanotube in Liquid with Tapping Mode AFM. *The 9th IEEE International Conference on Nano/Micro Engineered and Molecular Systems (NEMS)*; Waikiki Beach, HI, April 13−16, 2014; IEEE: Piscataway, NJ, 2014; pp 684−687.
(51) Ke, Y.; Castro, C.; Choi, J. H. Structural DNA Nanotechnology: Artificial Nanostructures for Biomedical Research. *Annu. Rev. Biomed. Eng.* **2018**, *20*, 375−401.
(52) Blanchard, A. T.; Salaita, K. Emerging Uses of DNA Mechanical Devices. *Science* **2019**, *365*, 1080.
(53) Wang, X.; Sha, R.; Kristiansen, M.; Hernandez, C.; Hao, Y.; Mao, C.; Canary, J. W.; Seeman, N. C. An Organic Semiconductor Organized into 3D DNA Arrays by "Bottom-up" Rational Design. *Angew. Chem., Int. Ed.* **2017**, *56*, 6445−6448.
(54) Aryal, B. R.; Ranasinghe, D. R.; Westover, T. R.; Calvopiña, D. G.; Davis, R. C.; Harb, J. N.; Woolley, A. T. DNA Origami Mediated Electrically Connected Metal—Semiconductor Junctions. *Nano Res.* **2020**, DOI: 10.1007/s12274-020-2672-5.
(55) Hui, L.; Xu, A.; Liu, H. DNA-Based Nanofabrication for Antifouling Applications. *Langmuir* **2019**, *35*, 12543−12549.

https://dx.doi.org/10.1021/acsnano.0c00178
ACS Nano XXXX, XXX, XXX−XXX